EXPERIMENTAL PULSED LASER, REMOTE CROSSWIND MEASUREMENT SYSTEM -- FEASIBILITY STUDY AND DESIGN. PART II

J. Fred Holmes, et al

Oregon Graduate Center

Prepared for:

Army Electronics Command

January 1975

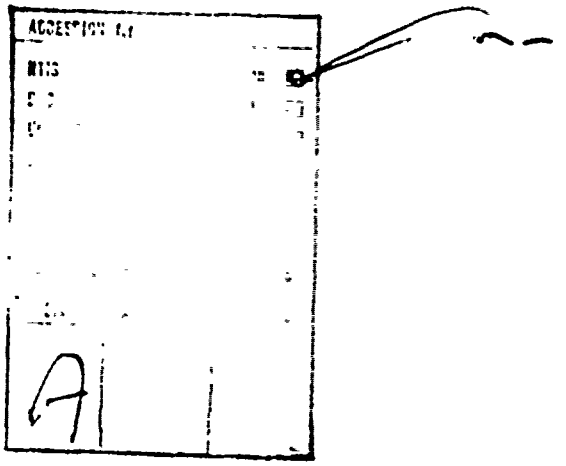

NOTICES

Disclaimers

The findings in this report are not to be construed as an official Department of the Army position, unless so designated by other authorized documents.

The citation of trade names and names of manufacturers in this report is not to be construed as official Government indorsement or approval of commercial products or services referenced herein.

Disposition

Destroy this report when it is no longer needed. Do not return it to the originator.

UNCLASSIFIED

SECURITY CLASSIFICATION OF THIS PAGE (When Data Entered)

REPORT DOCUMENTATION PAGE		READ INSTRUCTIONS BEFORE COMPLETING FORM
1 REPORT NUMBER ECOM75-1	2. GOVT ACCESSION NO.	3 RECIPIENT'S CATALOG NUMBER AD-A007 350
4 TITLE (and Subtitle) PULSED LASER, REMOTE CROSSWIND MEASUREMENT SYSTEM Feasibility Study and Design, Part II		5 TYPE OF REPORT & PERIOD COVERED Interim; 1 July 1974 - 31 December 1974 6 PERFORMING ORG. REPORT NUMBER
7 AUTHOR(s) J. Fred Holmes, J. Richard Kerr, Michael E. Fossey, R. Larry Jacob, Myung H. Lee		8 CONTRACT OR GRANT NUMBER(s) DAAD07-74-C-0094
9 PERFORMING ORGANIZATION NAME AND ADDRESS The Oregon Graduate Center 19600 N. W. Walker Road Beaverton, Oregon 97005		10. PROGRAM ELEMENT, PROJECT, TASK AREA & WORK UNIT NUMBERS
11 CONTROLLING OFFICE NAME AND ADDRESS U.S. Army Electronics Command, Atmospheric Sciences Laboratory, White Sands Missile Range, New Mexico		12. REPORT DATE January 1975 13. NUMBER OF PAGES 35
14 MONITORING AGENCY NAME & ADDRESS(if different from Controlling Office)		15. SECURITY CLASS. (of this report) Unclassified 15a. DECLASSIFICATION/DOWNGRADING SCHEDULE

16. DISTRIBUTION STATEMENT (of this Report)

Approved for public release; distribution unlimited.

17 DISTRIBUTION STATEMENT (of the abstract entered in Block 20, if different from Report)

18. SUPPLEMENTARY NOTES

19 KEY WORDS (Continue on reverse side if necessary and identify by block number)

Remote Crosswind Measurement, Remote Sensing, Laser Anemometer, Atmospheric Turbulence

20 ABSTRACT (Continue on reverse side if necessary and identify by block number)

The system analysis, design and construction of a sixty-four element, optical receiver for use with a double pulsed laser as a remote crosswind measurement system is described. In addition, formulations are developed for the mean square measurement error of the mean and variance resulting from estimating the statistics of the received intensity by a finite number of partially correlated samples, and from electronic noise. The results of the error analysis are applied to the case of a spherical wave.

DD FORM 1473 JAN 73 EDITION OF 1 NOV 65 IS OBSOLETE

UNCLASSIFIED PRICES SUBJECT TO CHANGE

SECURITY CLASSIFICATION OF THIS PAGE (When Data Entered)

Experimental Pulsed Laser, Remote Crosswind Measurement System -- Feasibility Study and Design (Part II)

J. Fred Holmes
J. Richard Kerr
Michael E. Fossey
R. Larry Jacob
Myung H. Lee

Contractor: Oregon Graduate Center for Study and Research

Sponsor: U. S. Army Electronics Command, Atmospheric Sciences Laboratory, White Sands Missile Range, New Mexico 88002

U. S. Air Force Weapons Laboratory
Kirtland Air Force Base, New Mexico 87117

Contract Number: DAA D07-74-C-0094

Effective Date of Contract: 1 July 1974

Contract Expiration Date: 30 June 1975

Amount of Contract: ECOM $92,055
AFWL $25,000

Principal Investigator: Dr. J. Richard Kerr

Co-Investigator: Dr. J. Fred Holmes

Project Monitor: Mr. Thomas H. Pries

CONTENTS

I. INTRODUCTION

This report describes the progress made during the period of the report on the feasibility study and design of an Experimental Pulsed Laser, Remote Cross Wind Measurement System. Work during the report period was concentrated on the analysis, design and construction of a sixty-four element optical receiver, described in Sections II and III, and an analysis of the accuracy of remote sensing measurements, described in Section IV.

II. RECEIVER ANALYSIS AND DESIGN

During the period of the report it was decided to replace the silicon vidicon tube, rotating disk receiver described in our last report[1] with a photodiode lens array receiver. This decision was based on problems encountered with the silicon vidicons.

The new receiver concept has many advantages including the ability to work off of a perfectly diffuse target, no moving parts, much closer resemblance to an actual field unit, direct adaptability to a 1.06 μm laser wavelength and a much lower transmitted energy requirement for a given signal to noise ratio.

The system design for the receiver is illustrated in Figures 2-1 and 2-2. The heart of the system is a unit cell that collects the ruby laser energy reflected from the target and provides an electrical signal suitable for storage and later processing. Sixty-four unit cells consisting of a plano-convex lens, two baffle plates, a photo detector, a current to voltage transducer and an integrate and hold amplifier are utilized in the system. The lenses are 22.4 mm in diameter with a 150 mm focal length and are arranged in a two-dimensional array with a center to center spacing of 30.48 mm.

There are several constraints on the lens spacing. Since we are basically measuring the covariance function with the instrument, the spacing should be such that three or four spacings span the

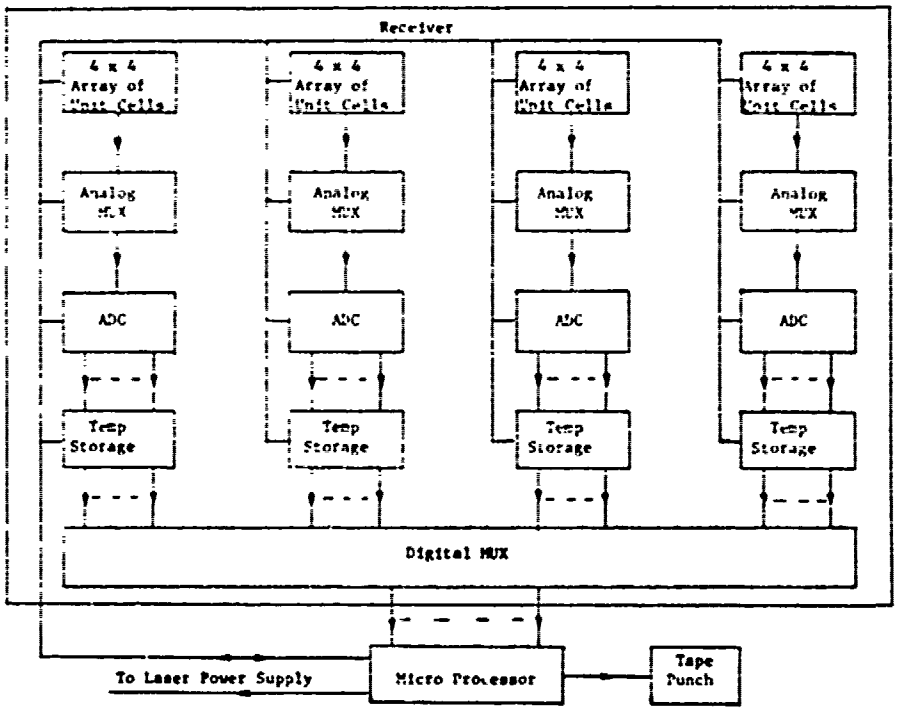

Figure 2-1 Receiver System Design

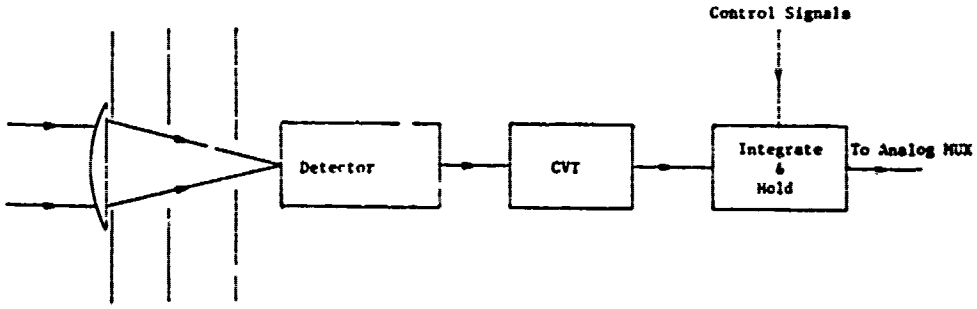

Figure 2-2 Unit Cell Design

majority of the covariance curve. Also, there are physical constraints on the total array size. From Figure 8 of our last report,[1] it appears that a total of around three Fresnel zones are required. The lens spacing in Fresnel zones of course depends on the range to the target. The spacing used in the system corresponds to 0.917 Fresnel zones at 1.6 Km and 0.67 Fresnel zones at 3.0 Km.

It is necessary to restrict the field of view (FOV) of each unit cell in order to limit the background light to an acceptable level. Care must be taken however to not overly restrict the FOV or fading due to angle of arrival fluctuation[2] may introduce errors into the measurements. Fortunately, neither an optical filter nor a precision FOV aperture is required. The lens in combination with the limited size of the active area on the detector limits the FOV and consequently the background to an acceptable level. The resultant FOV is approximately six milliradians.

The received background light has two deleterious effects. It acts as a bias that could saturate the unit cell if not restricted, and its fluctuations constitute a source of noise. Each of these effects is evaluated and a signal to noise ratio analysis for the unit cell is contained in Section III.

The photo current generated in the detector by the received laser pulse is amplified and converted to a voltage pulse by an operational amplifier operating in the current mode (refer to Figure 2-2). It is then integrated by the integrate and hold amplifier to provide an output proportional to the received energy in the pulse.

Electronically the system is divided into four independent modules, each containing a four by four array of unit cells, an analog multiplexer, a twelve bit analog to digital converter and a temporary storage means (refer to Figure 2-1). The outputs of each of the unit cells are sequentially multiplexed during the hold cycle to the analog to digital converter where the information is digitized and placed in temporary storage.

During normal operation of the system, a measurement cycle starts with the operator relinquishing control to the microprocessor. The microprocessor then charges the laser power supply and at the appropriate times provides signals to fire the laser flash lamp and Q switches, to integrate and hold and to transfer data. Each module goes through three complete cycles for each measurement. The first cycle occurs before the laser is fired and collects a set of data (64 numbers) representing background and offset in the integrators. The second and third cycles occur just after each of the two laser pulses respectively. After the end of the third module cycle, the data in temporary storage is transferred to the microprocessor. At the option of the operator it can be punched on paper tape. The operator also has the option of whether or not to subtract the background and offset data. The option was provided so that during alignment and test the subtraction process could be bypassed.

Timing of the Q switch pulses and the integrate cycles is crystal controlled. The delay time between flash lamp excitation and the first Q switch pulse is adjustable from 400 to 599 microseconds. The timing for the second Q switch pulse is designed to provide a fixed delay of one millisecond after the first Q switch pulse.

An analog output is provided to display the data collected on an oscilloscope. It can be used to preview a data set before deciding whether or not it should be punched and to verify that signal levels and alignment are proper.

An input connection is provided to allow an external unit cell to be used for recording the laser output energy on each pulse. This information is punched directly on the data tape and greatly simplifies calibration of the system.

The finished receiver is shown in Figures 2-3 through 2-6. The electronics fabrication was accomplished utilizing printed

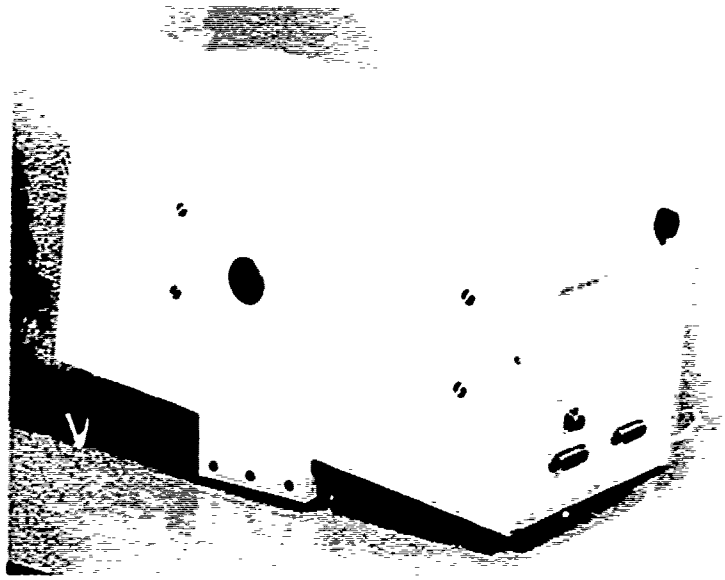

Figure 2-3 Receiver, Side View

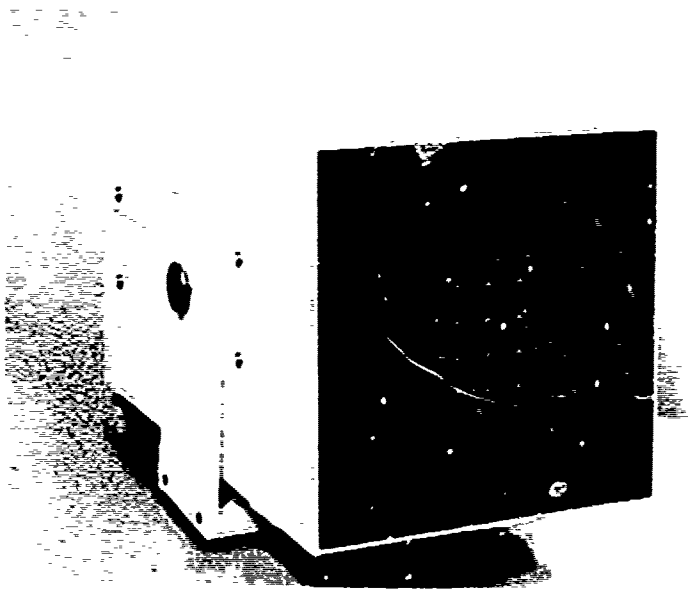

Figure 2-4 Receiver, Front View

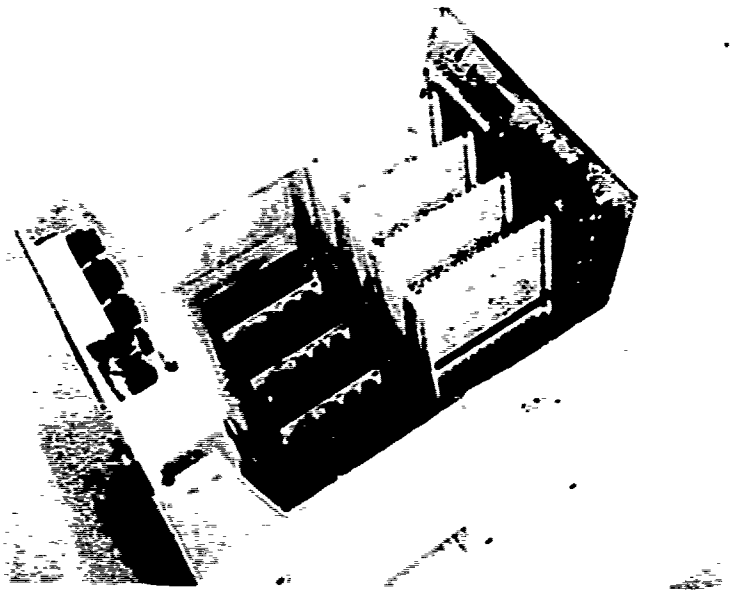

Figure 2-5 Receiver, Top View (cover removed)

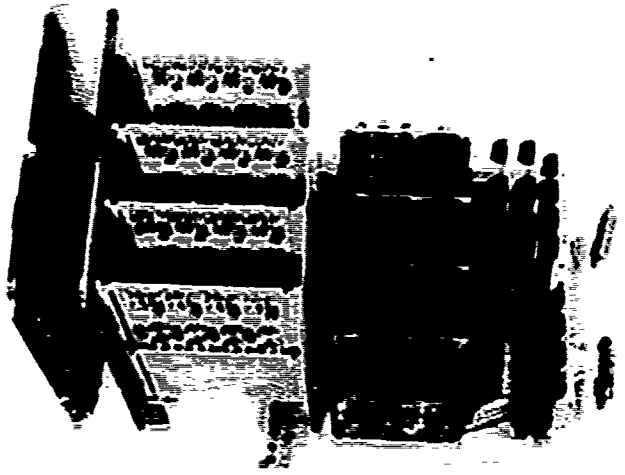

Figure 2-6 Receiver Electronics

circuit boards for the subassembly.

In addition a master printed circuit board utilizing an array of connectors was used to interconnect the various subassembly boards. This greatly reduces the amount of hand wiring and increases the reliability and maintainability of the system.

Regulated DC power and other interconnections enter the receiver through connectors on the back panel. Additional regulators on the circuit boards as well as RFI filters on the back panel are utilized to minimize interaction between the receiver and the laser power supply.

The receiver electronics are housed in an aluminum enclosure that is mounted in a cradle with two degrees of freedom. A telescope with crosshairs is mounted on the receiver and bore sighted with the optics to allow the receiver to be aimed at the target. A detailed description of the receiver circuitry will be published at a later date.

III. UNIT CELL ANALYSIS

In our last report,[1] it was noted that if a gated receiver is utilized, then for a given pulse energy, as the gate time is decreased, the signal to noise ratio (S/N) increases until signal shot noise limited operation is achieved. In addition, a crude estimate of the S/N versus gate time was developed. A much more exact analysis of the S/N versus gate time has been developed for the unit cell utilized in the new receiver and is presented in this section.

Figures 3-1 and 3-2 illustrate the electronics approach used in the unit cell design. A photodiode, operational amplifier combination operated in the current mode is utilized as a current to voltage transducer (CVT). The voltage output of this combination is then fed through a switch to an operational amplifier connected as an integrator. The capacitor used for integrating has a switch across it that is used to "dump" the accumulated charge after a measurement has been made. The integrator together with its switches will be treated as a single entity that acts like a "finite time integrator" (FTI).

The random process problem that we must solve is illustrated in Figure 3-3. The input random process $n(t)$ with autocorrelation function $R_{nn}(\tau)$ is wide sense stationary, "white" and represents any of the noise sources associated with the diode or the CVT. The impulse response $h_1(t)$ represents the linear circuitry between any of the noise sources and the output of the CVT. The exact forms will be considered later. The output $x(t)$ is then wide sense stationary with autocorrelation function $R_{xx}(\tau)$. The impulse response $h_2(t)$ of the finite time integrator is given by[3]

$$h_2(t) = G[u(t) - u(t-T)] \tag{3-1}$$

where G is a gain constant (1/RC) and $u(t)$ is the unit step function. In general, when a stationary process is sampled or

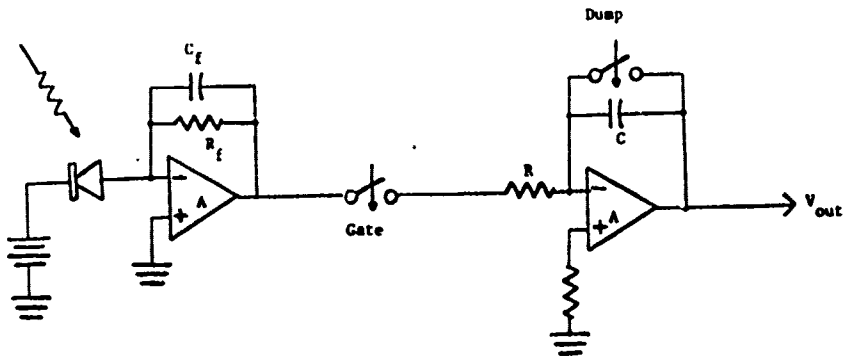

Finite Time Integrator

Fig. 3-1 Unit Cell Diagram

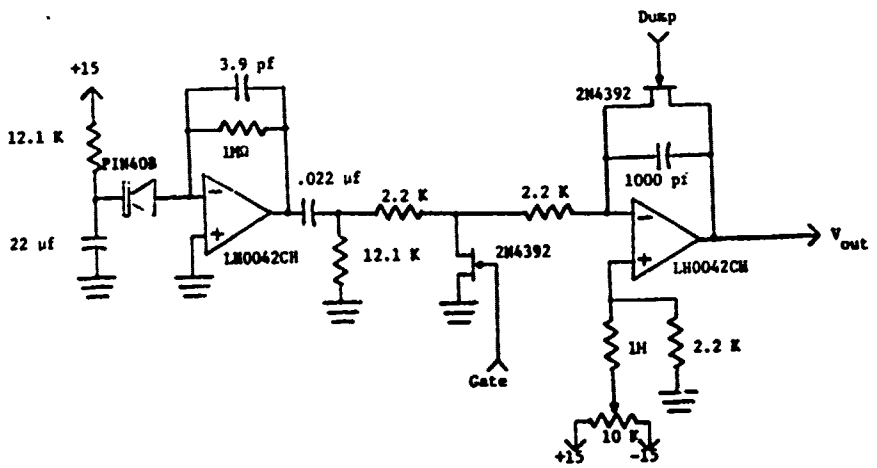

Fig. 3-2 Unit Cell Schematic

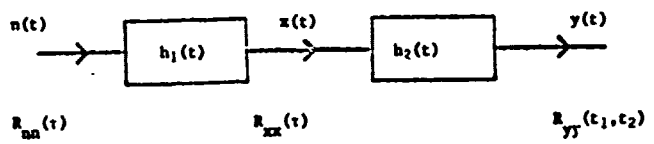

Fig. 3-3 Gated Stationary Process

switched, the output becomes non-stationary.[4] Consequently, analysis of the finite time integrator must be approached from the standpoint of a non-stationary process.

For a non-stationary process, the autocorrelation function at the output of a linear system is given by[4]

$$R_{yy}(t_2,t_1) = R_{yx}(t_2,t_1) * h_2(t_1) \tag{3-2}$$

where

$$R_{yx}(t_2,t_1) = R_{xx}(t_2,t_1) * h_2(t_1) \tag{3-3}$$

Working first with (3-3) and utilizing (3-1) it becomes

$$R_{yx}(t_2,t_1) = G \int_{-\infty}^{\infty} R_{xx}(t_2-\alpha)[u(t_1-\alpha) - u(t_1-\alpha-T)]d\alpha \tag{3-4}$$

where use has been made of

$$\tau = t_2 - t_1$$

Making the change of variable

$$P = t_2 - \alpha$$

(3-4) becomes

$$R_{yx}(t_2,t_1) = - G \int_{t_2-t_1}^{t_2-t_1+T} R_{xx}(P)dP = R_{yx}(t_2-t_1) \tag{3-5}$$

From (3-5) it is concluded that the cross correlation function $R_{yx}(t_2,t_1)$ is wide sense stationary.

Starting with (3-2) and utilizing the results of (3-5) and the same procedures it is found that

$$R_{yy}(t_2,t_1) = G \int_{-\infty}^{\infty} R_{yx}(\alpha-t_1)[u(t_2-\alpha) - u(t_2-\alpha-T)]d\alpha \tag{3-6}$$

Making the change of variable

$$Q = \alpha - t_1$$

$$R_{yy}(t_2,t_1) = G \int_{t_2-t_1}^{t_2-t_1-T} R_{yx}(Q)dQ = R_{yy}(t_2-t_1) \tag{3-7}$$

Consequently, the output of the finite time integrator is wide sense stationary which greatly simplifies the analysis.

Since the output y(t) is wide sense stationary, the variance can be expressed as[4]

$$\sigma_y^2 = \frac{1}{2\pi} \int_{-\infty}^{\infty} S_{yy}(\omega)d\omega \tag{3-8}$$

where

$$S_{yy}(\omega) = S_{nn}(\omega)\,|H_1(\omega)|^2\,|H_2(\omega)|^2 \tag{3-9}$$

and $H_1(\omega)$ and $H_2(\omega)$ are the Fourier transforms of the impulse responses $h_1(t)$ and $h_2(t)$ respectively. For the finite time integrator[3]

$$|H_2(\omega)|^2 = G^2 \frac{\mathrm{Sin}^2(\omega T/2)}{\left(\frac{\omega}{2}\right)^2} \tag{3-10}$$

However, $|H_1(\omega)|^2$ depends on which noise source is being evaluated. Assuming that each noise source is uncorrelated they may be analyzed separately and the results summed to give the total variance due to the noise sources. This yields[5]

$$\sigma_n^2 = \frac{1}{2\pi R^2 C^2} \int_{-\infty}^{\infty} \left[I_n^2|A(\omega)|^2 + \frac{4KT}{R_f}|B(\omega)|^2 + e_n^2|C(\omega)|^2\right] \frac{\mathrm{Sin}^2(\omega T/2)}{(\omega/2)^2}\, d\omega \tag{3-11}$$

where

$$|A(\omega)|^2 = \frac{R_f^2 \omega_n^4}{(\omega^2+\omega_n^2)^2} \tag{3-12}$$

$$|B(\omega)|^2 = \frac{R_f^2}{1+\omega^2 C_f^2 R_f^2} \tag{3-13}$$

$$|C(\omega)|^2 = \frac{e_n^4 [R_f/R_i+1]^2 [\omega^2 C_f^2 R_i^2/(R_f+R_i)^2 (C_i+C_f)^2 + 1]}{[\omega^2+\omega_n^2]^2} \tag{3-14}$$

$$I_n^2 = \frac{4KT}{r_d} + 2e(I_s+I_d+I_1+I_B) \tag{3-15}$$

e_n = Amplifier voltage noise $/\sqrt{Hz}$

r_d = Detector shunt resistance

R_1 = CVT amplifier input resistance

$$R_i = R_1 r_d/(R_1+r_d) \tag{3-16}$$

C_i = Total capacitance in shunt with CVT amplifier input terminals

$$\omega_n = [\omega_H/(R_f(C_i+C_f))]^{1/2} \tag{3-17}$$

ω_H = 2π · Gain-Bandwidth product of the amplifier

I_s = Signal Current

I_d = Detector dark current

I_B = Detector background current

and

I_1 = CVT amplifier input current

The parameters R, C and R_f are defined in Figure 3-1.

The expression given in (3-11) neglects any noise associated with the bias source and assumes that C_f is chosen for critically damped operation.

The signal to noise ratio at the output of the unit cell then is given by

$$S/N = \frac{V_{out}^2}{\sigma_n^2} \tag{3-18}$$

where V_{out} is the response of the unit cell to the signal. Since the signal current pulse is very short in comparison to the rise time of the amplifier, it behaves like an impulse. Consequently the output of the amplifier is just the impulse response of the network represented by (3-12). The output is given by

$$V(t) = -U_R \rho R_f \omega_n^2 t e^{-\omega_n t} u(t) \tag{3-19}$$

where U_R is the total received energy in the pulse and ρ is the diode responsivity in amps per watt. The voltage V(t) is integrated by the finite time integrator to yield

$$V_{out} = \frac{U_R \rho R_f \omega_n^2}{RC} \int_0^T t\, e^{-\omega_n t}\, dt \tag{3-20}$$

For T long compared to $1/\omega_n$, (3-20) becomes

$$V_{out} = \frac{\rho U_R R_f}{RC} \tag{3-21}$$

In order to calculate the signal to noise ratio, the signal and background levels must be evaluated. The received signal energy is given by

$$U_R = \frac{U_T T_R}{4} \left(\frac{D_L}{I}\right)^2 \tag{3-22}$$

where

U_T = Transmitted energy

T_R = Target reflectance

D_L = Receiver diameter in meters

and

L = Range to target in meters

Assuming a power incident on the target from the sun of 0.03 Watts/$Cm^2/\mu m$, the background power level is given by

$$P_B = \frac{3 \times 10^{-2} T_R}{16} [FOV \cdot D_L]^2 \, BW_o \qquad (3\text{-}23)$$

where

$FOV = D_d$/Focal Length

BW_o = Optical Bandwidth in μm

and

D_d = Diameter of detector active area

For the unit cell, the optical bandwidth is determined by the spectral response of the photodiode and is approximately 0.65 μm. Using a reflectivity of unity, this yields for the unit cell a background power level of approximately 0.7 microwatt. For a diode responsivity of 0.4 amps/watt and a one megohm feedback resistor this yields .28 μ amp for I_B and .28 volt for the output of the CVT.

The DC output due to background is not sufficient to saturate the CVT, but would cause a relatively large offset at the output of the integrator. To circumvent this problem, AC coupling and a "gate" switch was used between the CVT and the integrator. In picking the low frequency cutoff for the AC coupling, the frequency response of the CVT and signal must be considered. Figure 3-4 shows the impulse frequency response of the CVT. As can be seen from the figure, the low frequencies are important and consequently the cutoff for the AC coupling should be made as low as is practical. For the unit cell,

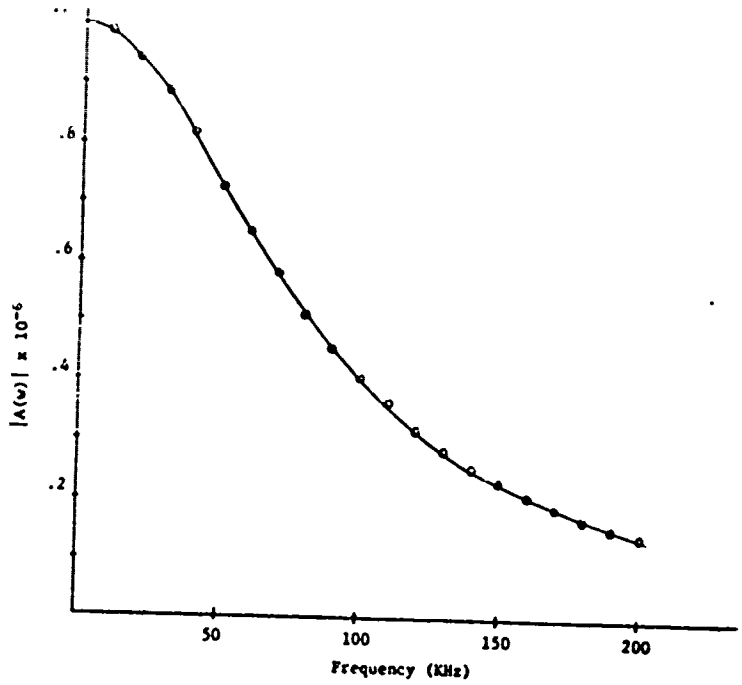

Figure 3-4 Impulse Frequency Response, CVT

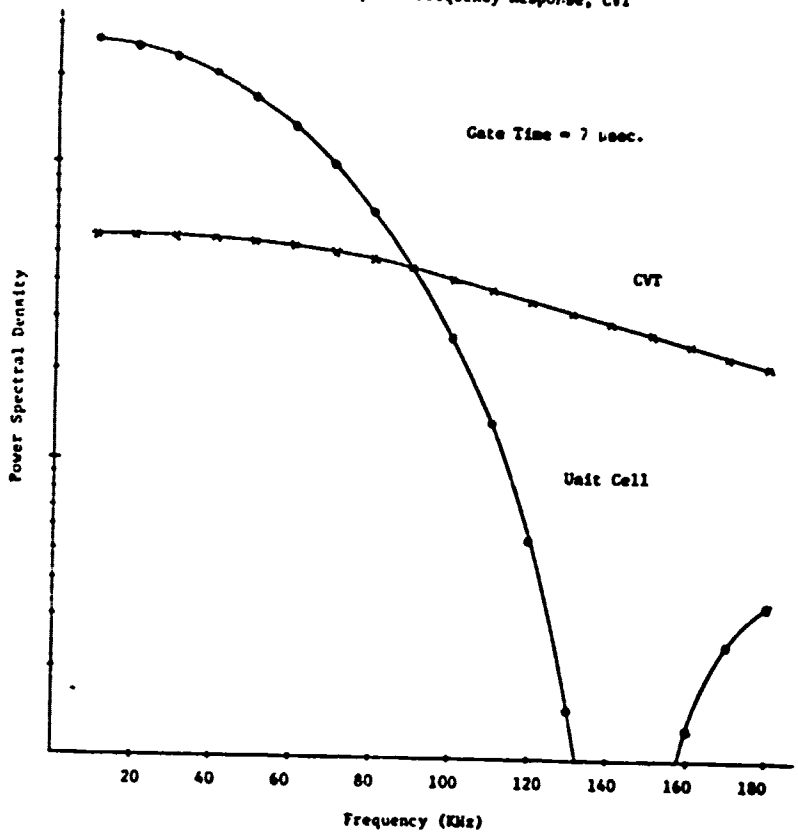

Figure 3-5 Output Power Spectral Density

the cutoff is approximately 2 KHz.

The power spectral density at the output of the CVT and the unit cell due to all the pertinent noise sources has been calculated in accordance with (3-9) through (3-16) and is shown in Figure 3-5. Utilizing (3-18), and (3-20) and the results illustrated in Figure 3-5, the signal to noise ratio for the unit cell has been calculated and is shown in Figure 3-6 versus gate time for a 0.1 reflectivity target[6] at 3 Km. For the present unit cell design, the optimum gate time is around six microseconds which yields a signal to noise ratio of approximately 53 db at a range of 3 Km. Both the gate delay time which compensates for signal time delay due to target range and the actual gate time are adjustable.

In the present unit cell design, the dominant noise sources are the CVT amplifier voltage noise and background current in the detector. Further improvement in the signal to noise ratio could be obtained by reducing these noise sources or by utilizing a shorter gate time. The latter approach would, however, require an amplifier with a wider bandwidth.

The unit cell design was tested with the ruby laser and good results were obtained. An oscilloscope picture of the output of the CVT is shown in Figure 3-7 for a diffuse target at 500 meters. The two superimposed traces correspond to the two laser output pulses.

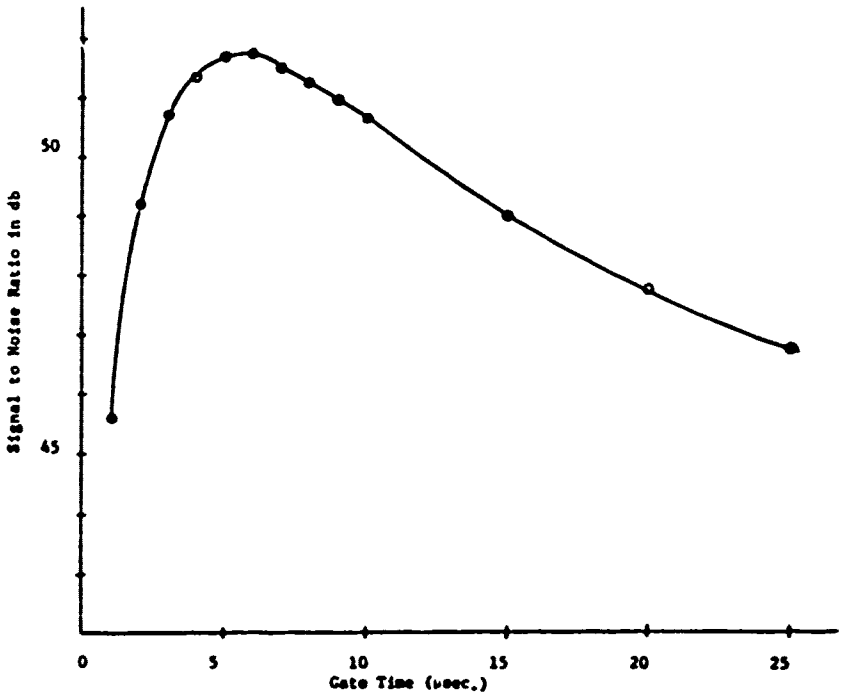

Figure 3-6 Signal to Noise Ratio Versus Gate Time

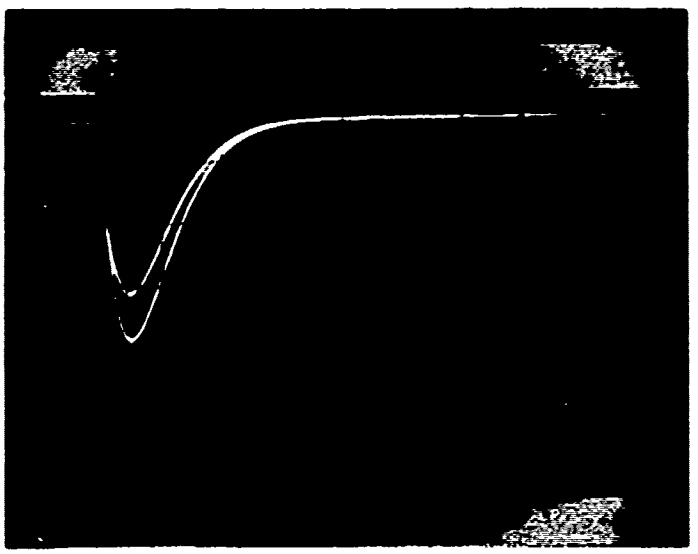

Figure 3-7 Pulse Response

IV. ACCURACY OF REMOTE SENSING MEASUREMENTS

There are several factors associated with remote sensing utilizing a pulsed laser system that will cause errors in evaluating the crosswind velocity and need to be investigated. These factors include a partially uncontrollable source size, saturation of the scintillations, receiver calibration, estimation of the statistics of the received intensity utilizing only a finite number of samples and electronic noise in the system.

As discussed in our last report,[1] the calibration constant that relates the measured slope of the covariance function to the path weighted average crosswind velocity is a function of the source size at the target end. Unfortunately the source size is a function of the turbulence level and the degree of coherence of the laser transmitter. The coherence of the laser transmitter will vary in an uncontrollable manner from measurement to measurement and from pulse to pulse in a single measurement. Preliminary analysis of the effect on the calibration constant indicates that as the source size increases, the sensitivity of the calibration constant to a changing source size decreases. This is illustrated in Figures 4-1 through 4-3. By proper choice of transmitter beam divergence and/or by estimating the source size from the measured data it should be possible to reduce the effect on crosswind measurement accuracy to a reasonable level. At this point the work has not proceeded far enough to warrant presenting a detailed analysis. This will be done in the final report for the year.

Saturation of the scintillations will cause the calibration constant to change with turbulence level. Work by NOAA[7] indicates that a proper choice of source and receiver sizes will minimize the effect. In addition, by estimating the degree of saturation from the measured data, it may be possible to compensate for the effects of saturation. Considerable additional work is required on this problem.

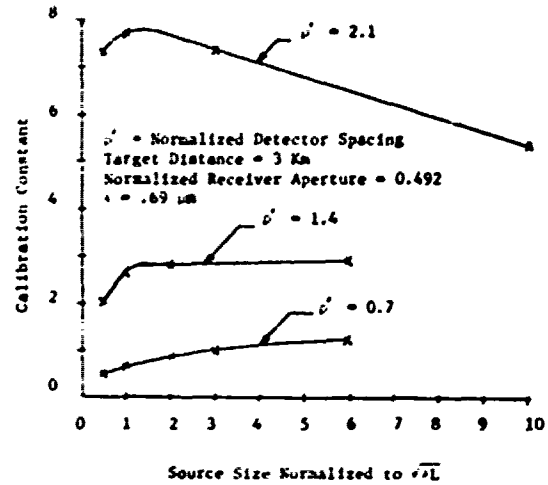

Figure 4-1 Calibration Constant, 3 Km

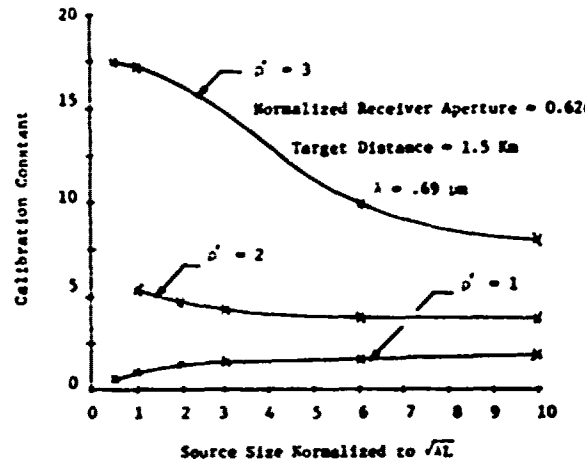

Figure 4-2 Calibration Constant, 1.6 Km

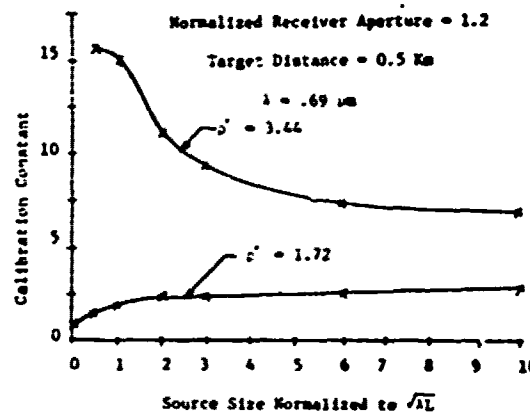

Figure 4-3 Calibration Constant, 0.5 Km

Each cell in the receiver array must be calibrated to compensate for variation of sensitivity from cell to cell. This is accomplished by utilizing a diffuse, poorly reflecting target at a range of about 500 feet. This provides a very nearly uniform illumination level to the receiver for calibration with a minimum of turbulence effects. Multiple sets of data are taken and processed on a digital computer to obtain calibration factors accurate to within a few percent.

Remote sensing by utilizing the effect of atmospheric turbulence on a propagating wave requires that certain statistical parameters be measured. For the specific case of crosswind measurement these parameters are the mean, variance, covariance function and slope of the covariance function. Due to constraints on the time allowed for the measurement and/or the number of spatial locations that can be utilized, these parameters must be estimated by utilizing a finite number of spatial and/or temporal samples. Consequently, this limits the accuracy with which the crosswind may be evaluated and in fact may be the limiting effect with respect to random errors.

In order to analyze the error due to using a finite number of samples, higher order joint moments of the intensity must be evaluated. Assuming that the joint distribution for the intensity is log-normal, the higher order moments may be evaluated in terms of the mean, variance and covariance. This is fortunate in that the higher order joint moments for the intensity have not in general been evaluated theoretically.

The joint moments to be evaluated are of the form

$$< I_1^{t_1} I_2^{t_2} \cdots I_n^{t_n} > = \int_{-\infty}^{\infty} \cdots \int_{-\infty}^{\infty} \alpha_1^{t_1} \alpha_2^{t_2} \cdots \alpha_n^{t_n} \, p_{\underline{I}}(\underline{\alpha}) \, d\alpha_1 \cdots d\alpha_n \qquad (4\text{-}1)$$

where $p_{\underline{I}}(\alpha)$ is the Nth order joint density function for the intensity and

$$N = \sum_{i=1}^{n} t_i$$

using

$$I_i = e^{x_i} \tag{4-2}$$

this can be expressed as

$$\langle I_1^{t_1} I_2^{t_2} \ldots I_n^{t_n} \rangle = \int_{-\infty}^{\infty} \ldots \int_{-\infty}^{\infty} e^{\alpha_1 t_1 + \alpha_2 t_2 \ldots + \alpha_n t_n} p_{\underline{x}}(\underline{\alpha}) d\alpha_1 \ldots d\alpha_n \tag{4-3}$$

where $p_{\underline{x}}(\underline{\alpha})$ is the multivariate jointly normal density function given by[8,9,10]

$$p_{\underline{x}}(\underline{\alpha}) = \frac{1}{(2\pi)^{n/2} [\text{Det } \underline{\lambda}]^{\frac{1}{2}}} e^{-\frac{1}{2}(\underline{\alpha} - \underline{\bar{x}})^{T} \underline{\lambda}^{-1} (\underline{\alpha} - \underline{\bar{x}})} \tag{4-4}$$

where

$$\underline{\lambda} = \begin{bmatrix} \lambda_{11} & \lambda_{12} \ldots & \lambda_{1n} \\ \lambda_{21} & & \\ \vdots & & \\ \lambda_{n1} \ldots & \ldots & \lambda_{nn} \end{bmatrix} \tag{4-5}$$

$$\underline{\alpha} = \begin{bmatrix} \alpha_1 \\ \alpha_2 \\ \cdot \\ \cdot \\ \cdot \\ \alpha_n \end{bmatrix} \tag{4-6}$$

$$\lambda_{ij} = \langle (x_i - \bar{x}_i)(x_j - \bar{x}_j) \rangle$$

$$\underline{\bar{x}} = \begin{bmatrix} \bar{x}_1 \\ \bar{x}_2 \\ \cdot \\ \cdot \\ \cdot \\ \bar{x}_n \end{bmatrix} \tag{4-7}$$

and $\bar{x}_i = \langle x_i \rangle$

Combining these, a rather general nth moment formulation for the intensity is obtained.

$$\langle I_1^{t_1} I_2^{t_2} \ldots I_n^{t_n} \rangle = \frac{1}{(2\pi)^{n/2}[\text{Det } \underline{\lambda}]^{\frac{1}{2}}} \int_{-\infty}^{\infty} \cdots \int_{-\infty}^{\infty} e^{\underline{t}^T \underline{\bar{x}}}$$

$$e^{-\frac{1}{2}(\underline{\alpha} - \underline{\bar{x}})^T \underline{\lambda}^{-1} (\underline{\alpha} - \underline{\bar{x}})} d\alpha_1 d\alpha_2 \ldots d\alpha_n \tag{4-8}$$

The evaluation of this integral[8] yields

$$\langle I_1^{t_1} I_2^{t_2} \ldots I_n^{t_n} \rangle = e^{\underline{t}^T \underline{\bar{x}} + \frac{1}{2} \underline{t}^T \underline{\lambda} \underline{t}} \tag{4-9}$$

which may be written in a slightly more usable form as

$$\langle I_1^{t_1} I_2^{t_2} \ldots I_n^{t_n} \rangle = e^{\sum_{i=1}^{n} t_i \bar{x}_i + \frac{1}{2} \sum_{i=1}^{n} \sum_{j=1}^{n} t_i \lambda_{ij} t_j} \tag{4-10}$$

This formulation for higher order moments of the intensity is expressed in terms of first and second moments of the log-intensity. With suitable manipulation it can however be expressed in terms of first and second moments of the intensity. Utilizing (4-10) to evaluate the first and second moments of the intensity yields

$$\langle I_i I_j \rangle = e^{\bar{x}_i + \bar{x}_j + \frac{1}{2}(\sigma_{x_i}^2 + 2\lambda_{ij} + \sigma_{x_j}^2)} \tag{4-11}$$

$$\langle I_i \rangle = e^{\bar{x}_i + \frac{1}{2}\sigma_{x_i}^2} \tag{4-12}$$

and

$$\langle I_i^2 \rangle = e^{2\bar{x}_i + 2\sigma_{x_i}^2} \tag{4-13}$$

which can be manipulated to generate

$$\left(\frac{\langle I_i^{t_i} \rangle}{\langle I_i^2 \rangle} \right)^{\frac{t_i}{2}} = e^{\bar{x}_i t_i} \tag{4-14}$$

and

$$\left(\frac{\langle I_i I_j \rangle}{\langle I_i \rangle \langle I_j \rangle} \right)^{\frac{t_i t_j}{2}} = e^{\frac{\lambda_{ij} t_i t_j}{2}} \tag{4-15}$$

Utilizing (4-14) and (4-15) in equation (4-10) yields

$$\langle I_1^{t_1} I_2^{t_2} \ldots I_n^{t_n} \rangle = \prod_{i=1}^{n} \left(\frac{\langle I_i \rangle^4}{\langle I_i^2 \rangle} \right)^{\frac{t_i}{2}} \prod_{i=1}^{n} \prod_{j=1}^{n} \left(\frac{C_{I_{i,j}}}{\langle I_i \rangle \langle I_j \rangle} + 1 \right)^{\frac{t_i t_j}{2}} \tag{4-16}$$

where

$$C_{I_{i,j}} = \langle (I_i - \bar{I}_i)(I_j - \bar{I}_j) \rangle$$

Equation (4-16) can be used to evaluate an Nth order joint moment of the intensity utilizing only the means, variances and covariances of the intensity. For the case where

$$\langle I_i \rangle = \langle I_j \rangle$$

$$\langle I_i^2 \rangle = \langle I_j^2 \rangle$$

this reduces to

$$\langle I_1^{t_1} I_2^{t_2} \ldots I_n^{t_n} \rangle = \left(\frac{\langle I \rangle^4}{\langle I^2 \rangle} \right)^{\frac{1}{2} \sum_{i=1}^{n} t_i} \left(\frac{\sigma_I^2}{\langle I \rangle^2} + 1 \right)^{\frac{1}{2} \sum_{i=1}^{n} t_i^2}$$

$$\prod_{\substack{i \neq j}}^{n} \prod^{n} \left(\frac{C_{I_{ij}}}{\langle I \rangle^2} + 1 \right)^{\frac{t_i t_j}{2}} \tag{4-17}$$

Formulations for the sampled mean, variance, covariance function and slope of the covariance function contained in our last report[1] are repeated here in a slightly modified form for convenience.

$$\bar{I} = \frac{1}{n^2} \left[\sum_{J=1}^{n} \sum_{K=1}^{n} I(J,K,L) \right] \tag{4-18}$$

$$\sigma_S^2 = \frac{1}{n^2} \left[\sum_{J=1}^{n} \sum_{K=1}^{n} [I(J,K,L) - \bar{I}]^2 \right] \tag{4-19}$$

$$C_{S_N}(ms',o) = \frac{1}{n\,\sigma_S^2}\left[\sum_{J=1}^{n}\left[\frac{1}{(n-m)}\sum_{K=1}^{n-m}[I(J,K,L)-\bar{I}][I(J,K+m,L)-\bar{I}]\right]\right] \tag{4-20}$$

$$M_{S_N}(ms') =$$

$$\frac{10^3}{n\,(n-m)\,\sigma_S(L=1)\,\sigma_S(L=2)}\sum_{J=1}^{n}\sum_{K=1}^{n-m}\Big[[I(J,K+m,2)-\bar{I}(L=2)]$$

$$[I(J,K,1)-\bar{I}(L=1)]-[I(J,K+m,1)-\bar{I}(L=1)][I(J,K,2)-\bar{I}(L=2)]\Big] \tag{4-21}$$

An analysis of the root-mean-square (RMS) error due to utilizing a finite number of samples to estimate the statistical parameters associated with the turbulence has been performed for the sample mean and sample variance. It is assumed that an n x n two-dimensional spatial or space-time array is used to collect the sampled values.

The mean square error for the sample mean can be expressed as

$$\langle(\bar{I}-\langle I\rangle)^2\rangle = \sigma_{\bar{I}}^2 = \langle(\bar{I})^2\rangle - (\langle I\rangle)^2 \tag{4-22}$$

Using equation (4-18) for the sample mean

$$\langle(\bar{I})^2\rangle = \frac{1}{n^4}\sum_{J1=1}^{n}\sum_{J2=1}^{n}\sum_{K1=1}^{n}\sum_{K2=1}^{n}\langle I(J1,K1)I(J2,K2)\rangle \tag{4-23}$$

which can be manipulated to yield

$$\langle(\bar{I})^2\rangle = \frac{1}{n^2}\langle I^2\rangle + \frac{1}{n^4}\sum_{J=1}^{n}\sum_{K1=1}^{n}\sum_{K2=1}^{n}\langle I(J,K1)I(J,K2)\rangle$$

$$(1-\delta_{K1,K2}) + \frac{1}{n^4}\sum_{J1=1}^{n}\sum_{K1=1}^{n}\sum_{J2=1}^{n}\sum_{K2=1}^{n}\langle I(J,K1)I(J2,K2)\rangle$$

$$(1-\delta_{J1,J2}) \tag{4-24}$$

Again using (4-22),

$$\langle \bar{I} \rangle^2 = \frac{1}{n^4} \left(\langle \sum_{J=1}^{n} \sum_{K=1}^{n} I(J,K) \rangle \right)^2 = \langle I \rangle^2 \qquad (4\text{-}25)$$

Combining (4-24) and (4-25) the mean square error for the sample mean becomes

$$\sigma_{\bar{I}}^2 = \frac{\sigma_I^2}{n^2} + \frac{1}{n^4} \sum_{J=1}^{n} \sum_{K1=1}^{n} \sum_{K2=1}^{n} C_I(J,K1,K2)(1-\delta_{K1,K2})$$

$$+ \frac{1}{n^4} \sum_{J1=1}^{n} \sum_{J2=1}^{n} \sum_{K1=1}^{n} \sum_{K2=1}^{n} C_I(J1,J2,K1,K2)(1-\delta_{J1,J2}) \qquad (4\text{-}26)$$

where the covariance C_I is given by

$$C_I(J1,J2,K1,K2) = \langle (I(J1,K1) - \langle I \rangle)(I(J2,K2) - \langle I \rangle) \rangle \qquad (4\text{-}27)$$

For the case of a spatial array with equal normalized spacing S' between cells this becomes

$$C_I(J1,J2,K1,K2) = C_I\left(S' \sqrt{(J1-J2)^2 + (K1-K2)^2}\right) \qquad (4\text{-}28)$$

Under this condition and after considerable manipulation the mean square error normalized to $\langle I \rangle^2$ becomes

$$\frac{\sigma_{\bar{I}}^2}{\langle I \rangle^2} = \frac{\sigma_I^2}{\langle I \rangle^2} \left[\frac{1}{n^2} + \frac{4}{n^3} \sum_{K=1}^{n-1} \left[(n-K) C_{I_N}(S'K) \right. \right.$$

$$\left. \left. + \frac{1}{n} \sum_{J=1}^{n-1} (n-J)(n-K) C_{I_N}\left(S' \sqrt{J^2 + K^2}\right) \right] \right] \qquad (4\text{-}29)$$

where C_{I_N} is the normalized covariance. The results of applying (4-29) to the case of a spherical wave[2] are illustrated in Figures 4-4 and 4-5. As can be seen from the figures, the error due to using a finite number of samples can be considerable. From (4-29) it can be seen that as the variance of the

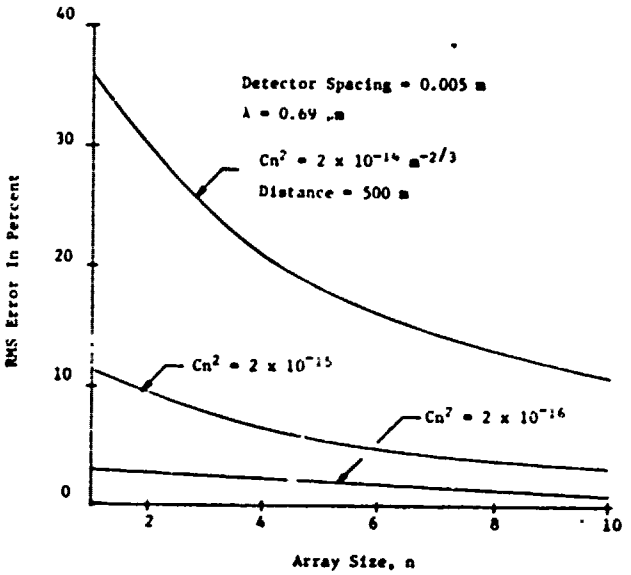

Figure 4-4 Normalized RMS Error, Sample Mean

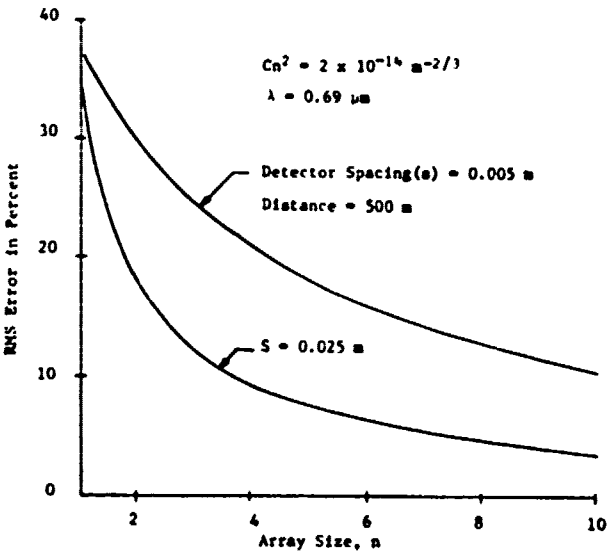

Figure 4-5 Normalized RMS Error, Sample Mean

intensity increases and as the covariance curve spreads out, the error for a given array size increases. Consequently, as the source size increases, the variance decreases lowering the error; however, the covariance curve spreads out,[1] thereby tending to increase the error. The covariance curve also spreads out[11] with increasing levels of saturation.

Equation (4-29) can also be used to evaluate the effect of electronic noise on the error. The electronic noise is composed of thermal noise, and Poisson fluctuations of bias current and signal current. The thermal and bias current noise is independent of the signal and its turbulence induced fluctuation and not correlated from cell to cell. This, however, is not the case for the shot noise associated with the signal. In order to simplify the analysis, it will however be assumed that the electronic noise and turbulence fluctuations are not correlated. With this assumption,

$$\sigma_I^2 \rightarrow \sigma_I^2 + \sigma_e^2$$

and

$$\langle I \rangle \rightarrow \langle I \rangle$$

where σ_e^2 is the variance due to electronic noise. This yields from (4-26)

$$\frac{\sigma_I^2}{\langle I \rangle^2} \rightarrow \frac{\sigma_e^2}{\langle I \rangle^2 n^2} + \frac{\sigma_I^2}{\langle I \rangle^2} = \frac{1}{n^2\ S/N} + \frac{\sigma_I^2}{\langle I \rangle^2} \qquad (4\text{-}30)$$

For this case, the errors due to the turbulence fluctuations and electronic noise add in the mean square sense. As an example and considering only the electronic noise, a signal to noise ratio of only 20 db and a 64 element array yields a normalized error due to electronic noise of only 1.25%

The normalized mean square error for the sample variance can be expressed as

$$\frac{\langle(\sigma_s^2 - \sigma_I^2)^2\rangle}{\sigma_I^4} = \frac{\langle\sigma_s^4\rangle}{\sigma_I^4} - 2\frac{\langle\sigma_s^2\rangle}{\sigma_I^2} + 1 \qquad (4\text{-}31)$$

Using equation 4-19 for the sample variance,

$$\langle\sigma_s^2\rangle = \sigma_I^2 - \bar{I}^2 \qquad (4\text{-}32)$$

and

$$\langle\sigma_s^4\rangle = \frac{1}{n^4}\sum_{J1=1}^{n}\sum_{J2=1}^{n}\sum_{K1=1}^{n}\sum_{K2=1}^{n}\langle I^2(J1,K1)I^2(J2,K2)\rangle$$

$$-\frac{2}{n^2}\langle\bar{I}^2\sum_J\sum_K I^2(J,K)\rangle + \langle\bar{I}^4\rangle \qquad (4\text{-}33)$$

where

$$\bar{I}^2 = \frac{1}{n^2}\sum_{J1=1}^{n}\sum_{K1=1}^{n}\sum_{J2=1}^{n}\sum_{K2=1}^{n} I(J1,K1)I(J2,K2) \qquad (4\text{-}34)$$

and

$$\bar{I}^4 = \frac{1}{n^8}\sum_{J1=1}^{n}\sum_{K1=1}^{n}\sum_{J2=1}^{n}\sum_{K2=1}^{n}\sum_{J3=1}^{n}\sum_{K3=1}^{n}$$

$$\sum_{J4=1}^{n}\sum_{K4=1}^{n} I(J1,K1)I(J2,K2)I(J3,K3)I(J4,K4) \qquad (4\text{-}35)$$

Combining (4-33) through (4-35) yields

$$\langle\sigma_s^4\rangle = \frac{1}{n^8}\sum_{J1,K1\ldots J4,K4=1}^{n}\langle I_1I_2I_3I_4\rangle$$

$$-\frac{2}{n^6}\sum_{J1,K1\ldots J3,K3=1}^{n}\langle I_1I_2I_3^2\rangle$$

$$+\frac{1}{n^4}\sum_{J1,K1,J2,K2=1}^{n}\langle I_1^2I_2^2\rangle \qquad (4\text{-}36)$$

The higher order moments of the intensity included in (4-36) can be evaluated utilizing (4-17). They are given by

$$\langle I_1 I_2 I_3 I_4 \rangle = \langle I \rangle^4 \left(\frac{C_{I_1 I_2}}{\langle I \rangle^2} + 1 \right) \left(\frac{C_{I_1 I_3}}{\langle I \rangle^2} + 1 \right) \left(\frac{C_{I_1 I_4}}{\langle I \rangle^2} + 1 \right)$$

$$\left(\frac{C_{I_2 I_3}}{\langle I \rangle^2} + 1 \right) \left(\frac{C_{I_2 I_4}}{\langle I \rangle^2} + 1 \right) \left(\frac{C_{I_3 I_4}}{\langle I \rangle^2} + 1 \right) \tag{4-37}$$

$$\langle I_1 I_2 I_3^2 \rangle = \langle I \rangle^4 \left(\frac{\sigma_I^2}{\langle I \rangle^2} + 1 \right) \left(\frac{C_{I_1 I_2}}{\langle I \rangle^2} + 1 \right) \left(\frac{C_{I_1 I_3}}{\langle I \rangle^2} + 1 \right)^2$$

$$\cdot \left(\frac{C_{I_2 I_3}}{\langle I \rangle^2} + 1 \right)^2 \tag{4-38}$$

and

$$\langle I_1^2 I_2^2 \rangle = \langle I \rangle^4 \left(\frac{\sigma_I^2}{\langle I \rangle^2} + 1 \right)^2 \left(\frac{C_{I_1 I_2}}{\langle I \rangle^2} + 1 \right)^4 \tag{4-39}$$

where

$$C_{I_1 I_2} = C_I \left(S' \sqrt{(J1-J2)^2 + (K1-K2)^2} \right) \tag{4-40}$$

etc.

Equation (4-31) in conjunction with (4-36) through (4-40) gives the normalized mean square error for the sample variance. The results of applying this to the case of a spherical wave[2] is illustrated in Figures 4-6 and 4-7. It is noted that the normalized sample error increases as the variance of the intensity increases and as the covariance increases. Therefore, the general discussion on the effect of source size, turbulence level and saturation on

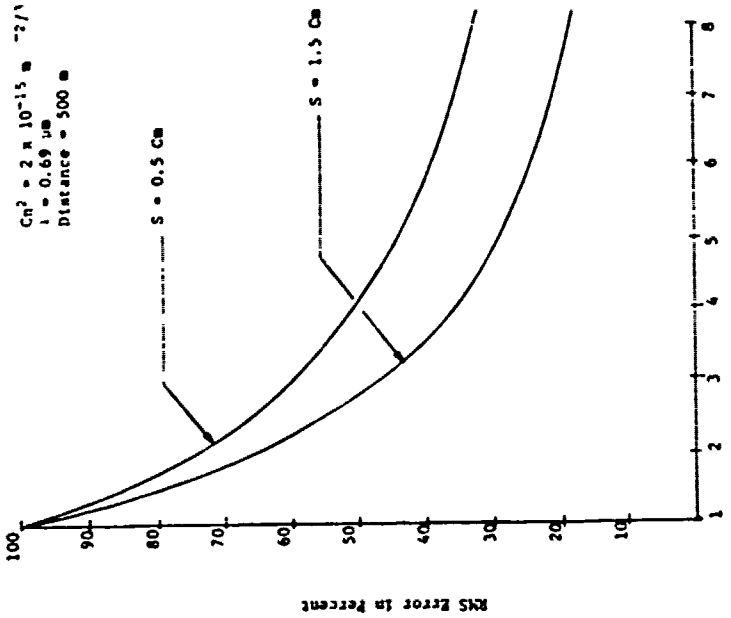

Figure 4-7 Normalized RMS Error, Sample Variance

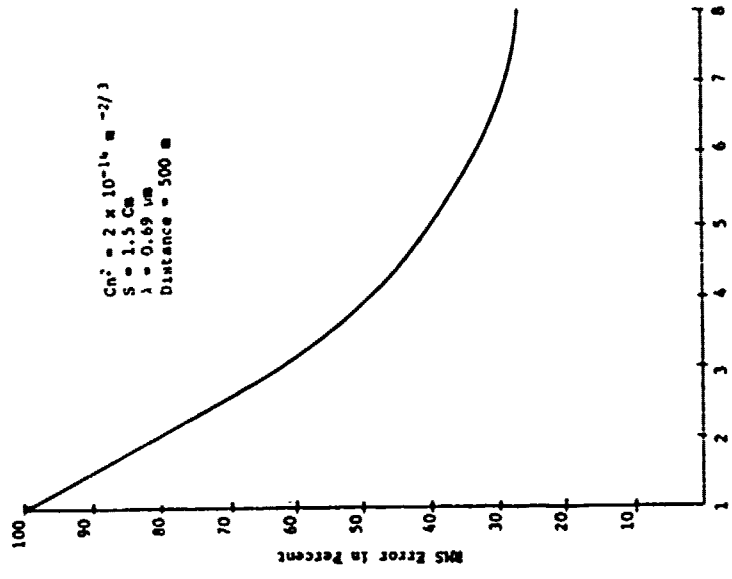

Figure 4-6 Normalized RMS Error, Sample Variance

the sample mean error also applies to the sample variance error.

The effect of electronic noise on the sample variance error can be evaluated using (4-31), (4-32), and (4-36). Again assuming no correlation between the turbulence fluctuations and the electronic noise

$$\langle \quad \rangle \rightarrow \langle \quad \rangle + \sigma_e^2 \left(1 - \frac{1}{n^2}\right) \tag{4-41}$$

and

$$\langle \quad \rangle \rightarrow \langle \quad \rangle + 2\left(1 + \frac{1}{n^2}\right) \quad \left(\quad - \quad \right) + \left(1 - \frac{1}{n^4} + \frac{2}{n^2}\right) \sigma_e^4 \tag{4-42}$$

The errors due to the turbulence fluctuations and electronic noise add in the mean square sense. The additional, normalized mean square error due to electronic noise is given by

$$2\left(1 + \frac{1}{n^2}\right) \frac{\sigma_e^2}{\sigma_I^2} + \left(1 - \frac{1}{n^4} + \frac{2}{n^2}\right) \frac{\sigma_e^4}{\sigma_I^4} - 2\left(1 + \frac{1}{n^2}\right) \frac{\sigma_e^2}{\sigma_I^2} \frac{\sigma_I^2}{\sigma_I^2}$$

$$- 2 \frac{\sigma_e^2}{\sigma_I^2} \left(1 - \frac{1}{n^2}\right) \tag{4-43}$$

As might be expected, the electronic contribution to the error increases as σ_I^2 decreases. Conversely the error due to turbulence fluctuations increases as σ_I^2 increases and the two effects compete. It is expected however that at reasonable electronic signal to noise ratios, the error due to turbulence fluctuations will dominate. Equation (4-43) can be simplified and put in terms of the electronic signal to noise ratio as follows:

$$\frac{4}{n^4}\frac{\sigma_I^2}{\sigma_I^2}\frac{1}{S/N} - 2\left(1+\frac{1}{n^2}\right)\frac{\sigma_I^2}{\sigma_I^2}\frac{\sigma_{\bar{I}}^2}{\sigma_I^2}\cdot\frac{1}{S/N}$$

$$+\left(1-\frac{1}{n^4}+\frac{2}{n^6}\right)\frac{\sigma_I^4}{\sigma_I^4}\frac{1}{(S/N)^2} \qquad (4\text{-}44)$$

The contribution of electronic noise to the normalized variance error is illustrated in Figures 4-8 and 4-9.

The analysis of errors associated with remote sensing of the crosswind is not yet completed. Remaining work includes formulating the same covariance error, sample slope of the covariance error and crosswind measurement error and applying it to the actual pulsed laser remote crosswind sensor configuration.

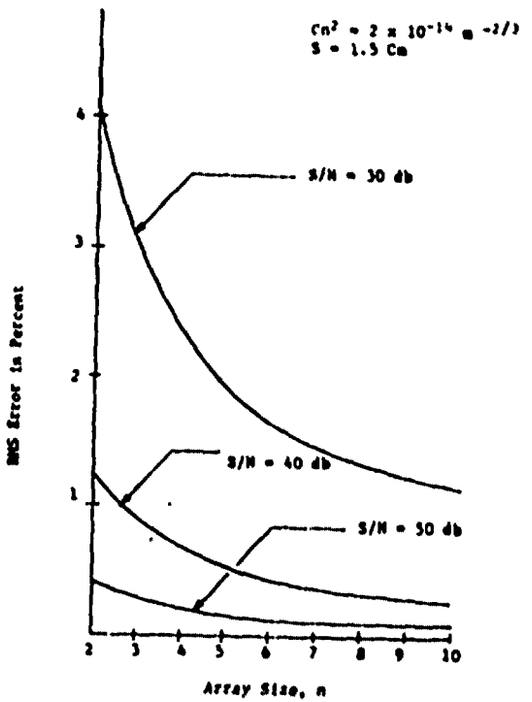

Figure 4-8 Normalized RMS Error, Electronic Noise, Sample Variance

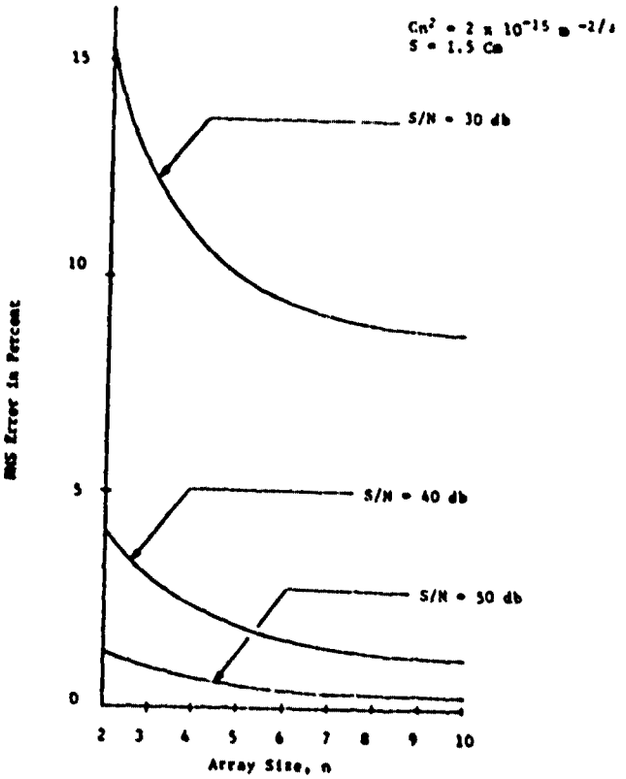

Figure 4-9 Normalized RMS Error, Electronic Noise

REFERENCES

1. Holmes, J. F. and J. R. Kerr, July 1974, "Experimental Pulsed Laser, Remote Crosswind Measurement System -- Feasibility Study and Design," U.S. Army Electronics Command, Research and Development Technical Report ECOM 74-0094-1, Atmospheric Sciences Laboratory, U.S. Army Electronics Command, White Sands Missile Range, New Mexico 88002.

2. Lawrence, R. S. and J. W. Strohbehn, 1970, "A Survey of Clean Air Turbulence Effects Relevant to Optical Communication," Proc. IEEE, 58, 1523.

3. Breipohl, A. M., Probabilistic Systems Analysis, John Wiley & Sons, New York.

4. Papoulis, A., 1965, Probability, Random Variables and Stochastic Processes, McGraw-Hill, New York.

5. Hamstra, R. H. and P. Wendland, 1972, "Noise and Frequency Response of a Silicon Photodiode Operational Amplifier Combination," Appl. Opt., 11, 1539.

6. Goldberg, I. I., November 1968, "Considerations of Automatic Tracker Application in Combat Vehicles," Department of the Army, Frankford Arsenal Memorandum Report M68-37-1, Philadelphia, Pa. 19137.

7. Clifford, S. F., G. R. Ochs, and Ting-i Wang, 1974, "Theoretical Analysis and Experimental Evaluation of a Prototype Passive Sensor to Measure Crosswinds," NOAA Technical Memorandum (Draft), NOAA, Boulder, Colorado.

8. Thomas, J. B., 1971, An Introduction to Applied Probability and Random Processes, John Wiley & Sons, New York.

9. Cramer, H., 1966, Mathematical Methods of Statistics, Princeton University Press, Princeton, New Jersey.

10. Wozencraft, J. M. and I. M. Jacobs, 1965, Principles of Communication Engineering, John Wiley & Sons, New York.

11. Clifford, S. F., et al, 1974, "Saturation of Optical Scintillation by Strong Turbulence," J. Opt. Soc. Am., 64, 148.